Impacts of Fluid Dynamics Simulation in Study of Nasal Airflow Physiology and Pathophysiology in Realistic Human Three-Dimensional Nose Models

De Yun Wang, MD[1] · Heow Peuh Lee, PhD[2] · Bruce R. Gordon, MD[3]

[1]Department of Otolaryngology, Yong Loo Lin School of Medicine, [2]Department of Engineering, Faculty of Engineering, National University of Singapore, Singapore; [3]Department of Otology and Laryngology, Massachusetts Eye and Ear Infirmary, Harvard Medical School, Boston and Division of Otolaryngology, Cape Cod Hospital, Hyannis, MA, USA

During the past decades, numerous computational fluid dynamics (CFD) studies, constructed from CT or MRI images, have simulated human nasal models. As compared to rhinomanometry and acoustic rhinometry, which provide quantitative information only of nasal airflow, resistance, and cross sectional areas, CFD enables additional measurements of airflow passing through the nasal cavity that help visualize the physiologic impact of alterations in intranasal structures. Therefore, it becomes possible to quantitatively measure, and visually appreciate, the airflow pattern (laminar or turbulent), velocity, pressure, wall shear stress, particle deposition, and temperature changes at different flow rates, in different parts of the nasal cavity. The effects of both existing anatomical factors, as well as post-operative changes, can be assessed. With recent improvements in CFD technology and computing power, there is a promising future for CFD to become a useful tool in planning, predicting, and evaluating outcomes of nasal surgery. This review discusses the possibilities and potential impacts, as well as technical limitations, of using CFD simulation to better understand nasal airflow physiology.

Key Words. *Computational fluid dynamics, Nose models, Nasal airflow dynamics, Airflow physiology and pathophysiology*

INTRODUCTION

The nasal cavity, with turbinates protruding from each lateral wall, is lined with pseudostratified columnar ciliated epithelium. Beneath the middle turbinates are the ostiomeatal complexes and outflow tracts from the anterior sinuses, and between the septum and the superior turbinates are the sphenoid outflow tracts. The physical shape of the nasal interior impacts significantly the important physiological functions of the nose, including air-conditioning, filtration, mucus flow, sinus drainage, and olfaction. Besides this, the nose also fulfills an important defense function as the first site of interaction with inhaled microbes, allergens, and chemicals. Critical to understanding all these nasal physiologic functions, is evaluating the pattern and intensity of inspiratory and expiratory airflow and how it interacts with the epithelium.

Standard rhinomanometry and acoustic rhinometry can determine changes in overall nasal airflow and resistance, and measure cross sectional areas in nasal cavity. However, due to the structural complexity of human noses, these studies are not able to show sufficient details of dynamic airflow through the nasal cavity to fully evaluate many intranasal conditions. However, these details can often be determined by modern computational fluid dynamics (CFD), which enables detailed study, and objective measurements, of airflow patterns within anatomically exact numerical human nose models. CFD studies have been reported that predict the airflow patterns and shear stress distribution, or study the effect of various anatomical factors on nasal patency. Examples include study of nasal airflow dynamics in nasal cavity [1-6], the relation between heat exchange and airflow patterns [7,8], odorant delivery [9-11], for dosimetry of inhalant gases [12], changed airflow dynamics in nasal septal deviation [13] or perforations [14-16] or nasal bone fracture [17],
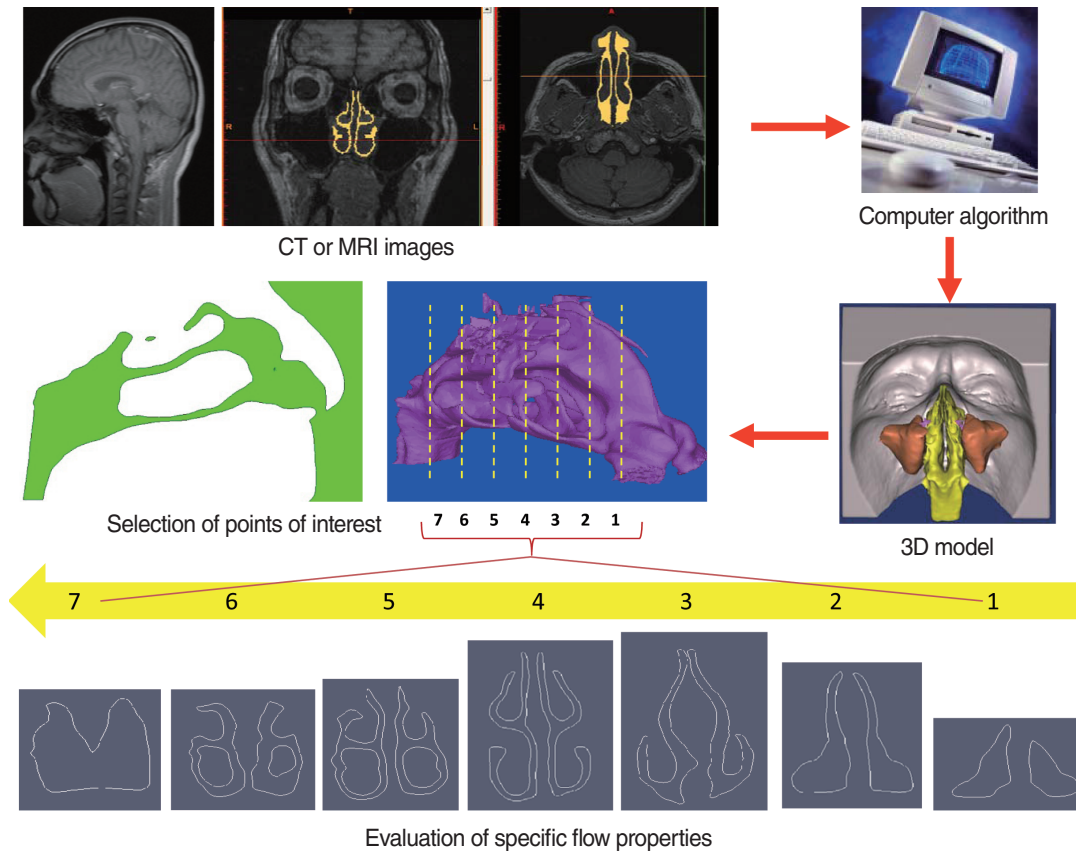
Fig. 1. Three-dimensional (3D) human nasal model can be constructed from a set of clinical imaging data, and used for computational fluid dynamics modeling calculations.

inferior turbinate hypertrophy [8,18,19] and aerodynamic effects of inferior turbinate surgery [20-22], after endoscopic sinus surgery [11,23,24], drug delivery and usage of intranasal medication [25-27].

Realistic, life-like CFD models are constructed from high-resolution clinical CT or MRI images using a commercial computer algorithm that converts scan data into a three-dimensional (3D) model (Fig. 1). Model outputs include airflow pattern (laminar or turbulent), velocity, pressure, wall shear stress, particle deposition, and temperature changes, at different flow rates, in different parts of the nasal cavity. The effects of both existing anatomical factors, as well as post-operative changes, can be assessed This review uses our previously published CFD study data as examples, and discusses the possibilities and potential impacts, as well as technical limitations, of using CFD simulation to better understand nasal airflow physiology.

CONSTRUCTION OF HUMAN NASAL MODEL AND CFD SIMULATION

The 3D nasal cavity model can be constructed from high-resolution MRI or CT images at intervals of 1.5 mm, or closer, in the axial plane. Segmentation is then performed using Mimics ver. 11 (Materialise, Leuven, Belgium; http://www.materialise.com/) resulting in a 3D nasal cavity model (Fig. 1). Smoothing for some of the highly corrugated surfaces is necessary before computational meshing, consequently, a locally developed algorithm is used for surface smoothing before performing CFD simulations. Despite smoothing, the main airway is properly captured in the 3D models, including accurate shapes of the inferior, middle, and superior turbinates and nasopharynx. CFD simulations are then performed using commercial software such as Fluent 6.3.22 (ANSYS Inc., Canonsburg, PA, USA; http://www.fluent.com/) or Adina (Adina R&D Inc., Watertown, MA, USA; http://www.adina.com/). The airflow is initially assumed to be incompressible, steady and laminar.

The choice of airflow rate in CFD simulation is important, as it is necessary to mimic as much as possible natural human breathing. Normally, inspiratory nasal airflow for an adult can range from 5 to 12 L/minute for calm breathing, and increases to 40 L/minute for physical exercise, with extreme airflow rates as large as 150 L/minute [28]. With such a range of flow rates, the Reynolds number (Re) can range from 4×10^2 to 1.2×10^4. Turbulent flow typically happens when Re is larger than 2×10^3, or 30 L/minute, inside a straight pipe. The onset of turbulence may oc-
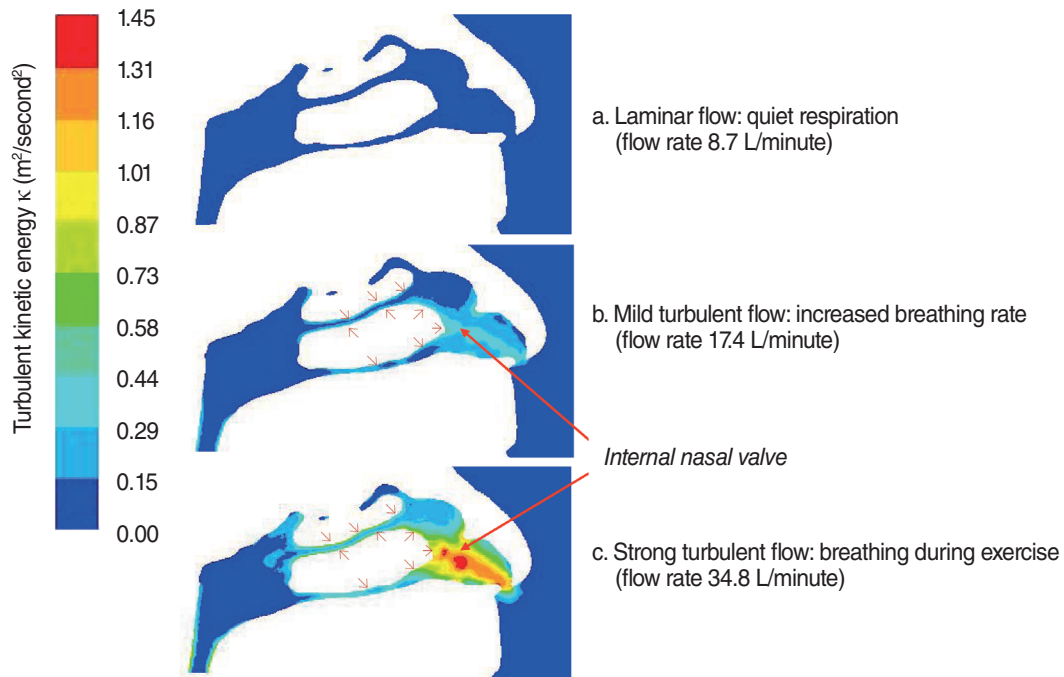
Fig. 2. Turbulent kinetic energy (m²/second²) airflow contours for a healthy nose with different flow rates. There is an obvious effect of airflow turbulence in maximizing air contact with the turbinate mucosa (small arrows).

cur at a lower *Re* in the complex geometries of the respiratory tract [29]. Moreover, with nasal obstruction, the cross section of the nasal cavity is decreased, which increases local flow rates and induces turbulence (Fig. 2). Thus, it is reasonable and necessary to implement a turbulent flow model for simulations with a large flow rate, such as 30 L/minute [19,21].
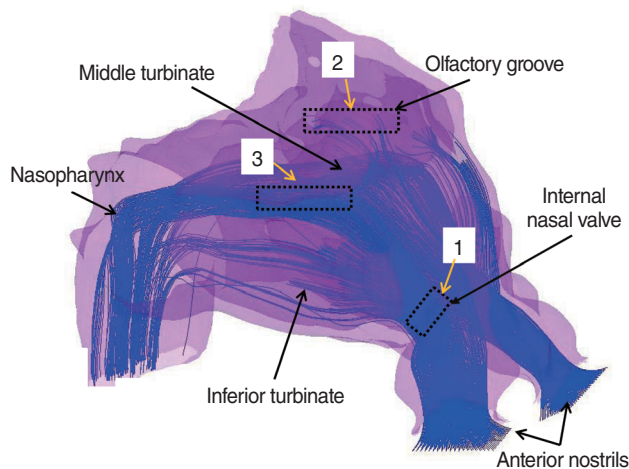
APPLIED AREAS

Significance of CFD study in understanding nasal airflow physiology

Previous studies have attempted to visualize the nasal valve region using endoscopy [30], acoustic rhinometry, and computed tomography [31], but none have been able to illustrate the relationship between form (anatomy) and function (physiology) as well as CFD models [6]. Our numerical study shows that in the healthy nose, the inspiratory airflow with the highest air speed is found in the anterior and middle airway, between the inferior and middle turbinates and the septum, and especially between the internal nasal valve and the anterior ends of the turbinates [18] (Figs. 2, 3). The pattern of this normal airflow largely depends on the function of the nasal valve, the primary airway resistor. The location of nasal valve has been described to occur at the entrance of the piriform aperture, the region just anterior to the tip of the inferior turbinate [32]. It is normally the narrowest region of the nasal passage, and, therefore, is a critically important functional region for nasal airflow [32,33]. In a healthy nose,

the nasal valve creates a zone of highly turbulent kinetic energy, high velocity, high negative pressure, and high wall shear stress (Figs. 2, 3). The nasal valve also changes the direction of the inspiratory air stream from the vestibule, and directs the bulk of airflow around the inferior turbinate. The aerodynamics of airflow changes significantly from a relatively laminar profile at the vestibule, to highly turbulent anterior to the head of the inferior turbinate. This is critical to facilitating mucosal contact for heating/cooling, humidification, and filtration of inspired air. This simple structure and the associated flow change, in conjunction with turbinate blood flow, gland function, and mucus transport, may explain directly the major physiologic function of the nose in conditioning inspired air.

Olfaction also depends on appropriate airflow past the olfactory epithelium at the apex of the nasal cavity. In the normal nose, the inspiratory air stream in the upper nose is low volume with low velocity and wall shear stress, and therefore, measureable durations for particle deposition, which could be the optimal condition for achieving good olfactory function (Fig. 3). However, in cases of moderate and severe nasal blockade, higher velocities and shear stresses, with negligible particle deposition times, is observed high in the nasal cavity, including the olfactory groove [18]. These changes in airflow could explain olfactory impairment in patients with persistent nasal obstruction due to turbinate hypertrophy.

The nasal cavity is able to condition (including both warming up and cooling down) inspiratory air to an optimal temperature before entering the lung. Our CFD study shows that anterior re-

Fig. 3. Three-dimensional (3D) model of inspiratory air streamlines (blue), with air velocity, pressure and wall shear stress measurements, at three points in both normal (healthy) and obstructed nose models. The flow rate used in computational fluid dynamics simulation is 34.8 L/minute.

Data points	Velocity (m/second)		Pressure (Pa)		Wall shear stress (Pa)	
	Normal	Obstructed	Normal	Obstructed	Normal	Obstructed
1	0.89	0.42	-16.68	-3.13	0.2	0.06
2	0.34	1.96	-12.08	-14.23	0.04	0.17
3	2.23	0.8	-13.56	-21.33	0.22	0.05

gions of the nasal cavity, especially around the inferior turbinate, are important for this function during inspiration [8]. In a healthy nose, the mucosa is able to heat inspired air from 5°C to 34°C. However, this warming is impaired in a nasal model with total inferior turbinectomy or a large reduction in the turbinate head.

Changes of airflow pattern in an anatomically abnormal nose

The nasal epithelium has a very complex vasculature, with a submucosal plexus of venous sinuses lining the nasal mucosa. These venous sinuses form erectile tissue that is well developed in the anterior part of the nasal septum, the inferior turbinate, and especially in the nasal valve region [34]. However, pathological enlargement of the inferior turbinates is a common mechanism of chronic nasal obstruction. The enlargement may be due to either the mucosal or osseous component, where the mean width has been reported to be nearly 11 mm when measured by CT [34,35]. In our CFD model, we were able to simulate turbinate enlargement by expanding the inferior turbinate homogenously outward by 1 and 2 mm to simulate moderate and severe nasal obstruction [18]. These degrees of obstruction can also be represented by an approximately one third reduction of the minimum cross-sectional area (MCA, 1.453 cm^2 in the healthy nose) for the moderate (0.873 cm^2) and two thirds (0.527 cm^2) for the severe nasal obstruction. This ratio of MCA reduction in moderate and severe obstruction is similar to what

was determined to occur during our previous study of nasal obstruction after nasal allergen challenge in allergic rhinitis patients [36].

From our CFD model of inferior turbinate hypertrophy, we were able to predict that the total nasal cavity pressure during inspiration is -10 Pa in a healthy nose, but -19 and -33 Pa in moderate and severe obstruction. The negative nasopharyngeal pressure induced by this nasal obstruction would be expected to impact soft palate function, and contribute to snoring and obstructive sleep apnea [18]. In addition, Eustachian tube function, important in the pathogenesis of middle ear disease, is affected by nasal obstruction. In our obstructing turbinate model, we observed a 4-fold higher air velocity, and negative pressure (-35%), at the Eustachian tube orifice [18], factors that are likely to be important for tubal function.

Turbinate reduction surgery may be indicated for inferior turbinate enlargement when conservative treatment fails. Using CFD simulations, we were able to quantitatively evaluate the effects of inferior turbinate surgery on nasal aerodynamics in a series of CFD models of the normal nose, nose with enlarged inferior turbinates [18], and the same nose after three surgical procedures: 1) resection of the lower third of the inferior turbinate, 2) excision of the head of the inferior turbinate, and 3) radical inferior turbinate resection. The results show that in the normal nose, the bulk of air streamlines traversed the common meatus between the inferior and middle turbinates in a relatively vortex-free flow. When the inferior turbinate is enlarged, the streamlines are directed superiorly at higher velocity, and wall shear stress in the nasopharynx is increased. Of the three simulated surgical techniques, wall shear stress and intranasal pressures achieved near-normal levels after resection of the lower third, but not in the other two surgical models. The airflow patterns and pressures obtained following radical turbinate resection were comparable to a previously published CFD study on a patient suffering with debilitating atrophic rhinitis, where the airstreams were disorganized and turbulent, resulting in minimal contact with the remaining nasal mucosa [37]. Furthermore, insufficient warming of inspired air was also demonstrated [8].

We have also studied airflow patterns in the presence of septal deviation, septal perforation, and nasal bone fracture in our CFD simulations [13,16,17]. In these studies, we were able to show major changes qualitatively and quantitatively in the pattern of inspiratory airflow (e.g., flow partitioning and airway resistance, velocity distribution, and intensity and location of turbulence), wall shear stress, and increased of total negative pressure through the nasal cavity. For example, the functional nasal valve region becomes less apparent or even disappeared in these pathological conditions.

Aerodynamic changes after functional endoscopic sinus surgery

Existence of airflow circulation or re-circulation inside the main

nasal cavity volume was found in healthy nasal models [1,38,39]. However, airflow going into the sinuses is negligible for a healthy nose, and this restricted amount of air exchange by the sinuses, through their ostia, helps to maintain stable intrasinus nitric oxide (NO) and humidity levels [40,41]. The sinuses produce NO [42], and a stable concentration is needed to maintain a sterile local environment and optimal host defense and local immunologic reactions [42,43]. Xiong et al. [44] found, by CFD simulation, that in the post-functional endoscopic sinus surgery (FESS) model, there was an increase in airflow and air exchange in the maxillary, ethmoid and sphenoid sinuses, with a 13% increase of airflow through the area connecting the middle meatus and the surgically opened ethmoid. Similarly, our CFD study confirmed significantly increased airflow intensity, with turbulence, inside the maxillary sinus with an enlarged ostium after FESS [27]. The uncinate process may have a protective role in preventing deposition of bacteria and allergens into the sinuses during the inspiration. After standard FESS, with the removal of the uncinate and widening of ostia, the existence of continuous airflow circulation inside the sinuses may affect both local NO concentrations and deposition of bacteria and allergens into the sinus cavities [45,46].

CFD simulation for intranasal drug delivery

Intranasal medications, such as intranasal corticosteroids (INSs), a standard treatment for allergic rhinitis and rhinosinusitis, are commonly used in treating nasal diseases [47,48]. There have been some studies to quantify the impact of nasal obstruction [49,50] and head position [51] on INS deposition. Because these studies were small, and most were performed in healthy subjects, the results are inconclusive. In educational materials provided by INS-producing companies, various head positions are recommended for nasal drug use. However, not all these head positions are easily performed, nor well-supported by objective data. Our CFD study results demonstrate that there is no significant effect of head positions between 0° and 90° on drug flow through the nasal valve region [25]. As expected, moderate or severe nasal obstruction, due to inferior turbinate hypertrophy, decreases drug penetration rates (80.97-82.13%, 8.08-8.37%, and 0.21-0.27% in the healthy, moderately, and severely obstructed nose, respectively). We also found drug penetration increased by 10 to 20-fold in the presence of inspiratory airflow, when compared to no airflow (0-8.81%) [25]. Therefore, it is advisable to have both a steady, moderate inspiratory airflow and no obstruction in order to optimize INS particle deposition [25,26].

TECHNICAL LIMITATIONS OF CFD SIMULATION STUDIES

It can be argued that CFD studies are only simulations, and the predicted results are derived from complex calculations of the Navier-Stokes equation, which may not represent real life conditions. In the simulations, air is routinely regarded as being incompressible, in order that fluid dynamic theories will be easily applicable. This assumption is acceptable given that the pressure changes within the nasal cavity are small. Secondly, the aerodynamics of nasal airflow is complex due to the geometry of the nasal cavity. Unlike a smooth, incompressible tube, the nature of nasal airflow (laminar, turbulent or semi-turbulent) in different parts of nasal cavity varies due to the changes in surface structures, which requires some mathematical smoothing to enable simulation. As computer processing improves, closer approximations to the precise nasal contours will be able to be ever more accurately reflected in better 3D models. Already, however, the CFD models produce realistic models which agree with other methods of observing nasal air flow, and produce consistent, understandable results.

FUTURE STUDIES

Anatomical variations of the nasal cavity from person to person may also cause changes in the flow pattern of the nasal cavity. For example, a previous numerical study [1], found the highest inspiratory air speed was along the nasal floor, below the inferior turbinate, with a second, lower, peak occurred in the middle of the airway, between the inferior and middle turbinates and the septum, where we identified the maximum flows. This difference could be due to various factors. For example, different ethnic groups have evolved variant nasal morphologies under varied climactic conditions, which may result in nasal airflow variations and differing optimums and/or ranges of nasal functions. For example, we recently compared CFD simulations of nasal airflow patterns to understand the consequences of different nasal morphology between three subjects from Caucasian, Chinese, and Indian ethnic groups. The results show that more airflow passes through the middle part of the nasal airway in the Caucasian model, and more through the inferior part in the Indian model, as compared to the Chinese model [52]. The Indian model also showed extremely low flows through the olfactory region. However, more CFD studies are needed in different racial groups in order confirm and extend these pioneering data.

It is suggested by a recent study that virtual nasal surgery has the potential to be a predictive tool that will enable surgeons to perform personalized nasal surgery using computer simulation techniques [53]. Similarly, assessment of nasal function has also been shown to be evolving with the introduction of CFD techniques, which allow for a detailed description of the biophysics of nasal airflow that have the potential to change the way we assess nasal form and function [54]. Therefore, in the future, CFD studies may be useful in clinical situations, such as predicting the degree of functional impairment due to injury or ana-

tomic variations, and could help in determining the need for surgery, for surgical planning of corrections for inferior turbinate hypertrophy and other nasal anatomical malformations, and to evaluate the results of surgery or degree of disability. For this work, specialized CFD simulation software needs to be developed.

CONCLUSION

Modern CFD technology enables detailed study and objective measurements of many important physical characteristics of the airflow within anatomically accurate human nasal models, constructed from CT or MRI images. Although the results from CFD study are derived from complex calculations which may not exactly represent real life conditions, these simulations provide clinically useful, logically consistent, and understandable information that standard rhinomanometry and acoustic rhinometry cannot. CFD allows visual appreciation of nasal airflow, including airflow streamline patterns (with laminar or turbulent flow), velocity, pressure, wall shear stress, particle deposition, and temperature changes, under different flow rate conditions in different parts of nasal cavity. The effect of various anatomical variants, such as septal deviation or perforation, turbinate hypertrophy, and prior injury or surgery can all be easily visualized, and the effects on physiologic functioning can be appreciated. With expected improvements in CFD technology and computing power, there is a promising future for this technique to become a useful tool for evaluating degree of dysfunction, planning nasal surgery predicting outcomes, and evaluating surgical results.

CONFLICT OF INTEREST

No potential conflict of interest relevant to this article was reported.

ACKNOWLEDGMENTS

REFERENCES

1. Keyhani K, Scherer PW, Mozell MM. Numerical simulation of airflow in the human nasal cavity. J Biomech Eng. 1995 Nov;117(4):429-41.
2. Castro Ruiz P, Castro Ruiz F, Costas Lopez A, Cenjor Espanol C. Computational fluid dynamics simulations of the airflow in the human nasal cavity. Acta Otorrinolaringol Esp. 2005 Nov;56(9):403-10.
3. Martonen TB, Quan L, Zhang Z, Musante CJ. Flow simulation in the human upper respiratory tract. Cell Biochem Biophys. 2002;37(1):27-36.
4. Weinhold I, Mlynski G. Numerical simulation of airflow in the human nose. Eur Arch Otorhinolaryngol. 2004 Sep;261(8):452-5.
5. Horschler I, Schroder W, Meinke M. On the assumption of steadiness of nasal cavity flow. J Biomech. 2010 Apr;43(6):1081-5.
6. Leong SC, Chen XB, Lee HP, Wang DY. A review of the implications of computational fluid dynamic studies on nasal airflow and physiology. Rhinology. 2010 Jun;48(2):139-45.
7. Pless D, Keck T, Wiesmiller K, Rettinger G, Aschoff AJ, Fleiter TR, et al. Numerical simulation of air temperature and airflow patterns in the human nose during expiration. Clin Otolaryngol Allied Sci. 2004 Dec;29(6):642-7.
8. Chen XB, Lee HP, Chong VF, Wang de Y. Numerical simulation of the effects of inferior turbinate surgery on nasal airway heating capacity. Am J Rhinol Allergy. 2010 Sep-Oct;24(5):e118-22.
9. Keyhani K, Scherer PW, Mozell MM. A numerical model of nasal odorant transport for the analysis of human olfaction. J Theor Biol. 1997 Jun;186(3):279-301.
10. Zhao K, Scherer PW, Hajiloo SA, Dalton P. Effect of anatomy on human nasal air flow and odorant transport patterns: implications for olfaction. Chem Senses. 2004 Jun;29(5):365-79.
11. Zhao K, Pribitkin EA, Cowart BJ, Rosen D, Scherer PW, Dalton P. Numerical modeling of nasal obstruction and endoscopic surgical intervention: outcome to airflow and olfaction. Am J Rhinol. 2006 May-Jun;20(3):308-16.
12. Kimbell JS, Subramaniam RP. Use of computational fluid dynamics models for dosimetry of inhaled gases in the nasal passages. Inhal Toxicol. 2001 May;13(5):325-34.
13. Chen XB, Lee HP, Chong VF, Wang DY. Assessment of septal deviation effects on nasal air flow: a computational fluid dynamics model. Laryngoscope. 2009 Sep;119(9):1730-6.
14. Grant O, Bailie N, Watterson J, Cole J, Gallagher G, Hanna B. Numerical model of a nasal septal perforation. Stud Health Technol Inform. 2004;107(Pt 2):1352-6.
15. Pless D, Keck T, Wiesmiller KM, Lamche R, Aschoff AJ, Lindemann J. Numerical simulation of airflow patterns and air temperature distribution during inspiration in a nose model with septal perforation. Am J Rhinol. 2004 Nov-Dec;18(6):357-62.
16. Lee HP, Garlapati RR, Chong VF, Wang DY. Effects of septal perforation on nasal airflow: computer simulation study. J Laryngol Otol. 2010 Jan;124(1):48-54.
17. Chen XB, Lee HP, Chong VF, Wang DY. Assessments of nasal bone fracture effects on nasal airflow: a computational fluid dynamics study. Am J Rhinol Allergy. 2011 Jan-Feb;25(1):e39-43.
18. Lee HP, Poh HJ, Chong FH, Wang de Y. Changes of airflow pattern in inferior turbinate hypertrophy: a computational fluid dynamics model. Am J Rhinol Allergy. 2009 Mar-Apr;23(2):153-8.
19. Chen XB, Lee HP, Chong VF, Wang DY. Impact of inferior turbinate hypertrophy on the aerodynamic pattern and physiological functions of the turbulent airflow: a CFD simulation model. Rhinology. 2010 Jun;48(2):163-8.
20. Wexler D, Segal R, Kimbell J. Aerodynamic effects of inferior turbinate reduction: computational fluid dynamics simulation. Arch Otolaryngol Head Neck Surg. 2005 Dec;131(12):1102-7.
21. Chen XB, Leong SC, Lee HP, Chong VF, Wang DY. Aerodynamic effects of inferior turbinate surgery on nasal airflow: a computational fluid dynamics model. Rhinology. 2010 Dec;48(4):394-400.
22. Lee HP, Garlapati RR, Chong VF, Wang DY. Comparison between effects of various partial inferior turbinectomy options on nasal airflow: a computer simulation study. Comput Methods Biomech Biomed Engin. 2011 Sep 14 [Epub]. http://dx.doi.org/10.1080/10255842.2011.609481.

23. Lindemann J, Brambs HJ, Keck T, Wiesmiller KM, Rettinger G, Pless D. Numerical simulation of intranasal airflow after radical sinus surgery. Am J Otolaryngol. 2005 May-Jun;26(3):175-80.

24. Chen XB, Lee HP, Chong VF, Wang DY. Aerodynamic characteristics inside the rhino-sinonasal cavity after functional endoscopic sinus surgery. Am J Rhinol Allergy. 2011 Nov-Dec;25(6):388-92.

25. Garlapati RR, Lee HP, Chong FH, Wang DY. Indicators for the correct usage of intranasal medications: a computational fluid dynamics study. Laryngoscope. 2009 Oct;119(10):1975-82.

26. Chen XB, Lee HP, Chong VF, Wang DY. A computational fluid dynamics model for drug delivery in a nasal cavity with inferior turbinate hypertrophy. J Aerosol Med Pulm Drug Deliv. 2010 Oct;23(5):329-38.

27. Chen XB, Lee HP, Chong VF, Wang DY. Drug delivery in the nasal cavity after functional endoscopic sinus surgery: a computational fluid dynamics study. J Laryngol Otol. 2012 May;126(5):487-94.

28. Hooper RG. Forced inspiratory nasal flow-volume curves: a simple test of nasal airflow. Mayo Clin Proc. 2001 Oct;76(10):990-4.

29. Lin CL, Tawhai MH, McLennan G, Hoffman EA. Characteristics of the turbulent laryngeal jet and its effect on airflow in the human intra-thoracic airways. Respir Physiol Neurobiol. 2007 Aug;157(2-3):295-309.

30. Suh MW, Jin HR, Kim JH. Computed tomography versus nasal endoscopy for the measurement of the internal nasal valve angle in Asians. Acta Otolaryngol. 2008 Jun;128(6):675-9.

31. Terheyden H, Maune S, Mertens J, Hilberg O. Acoustic rhinometry: validation by three-dimensionally reconstructed computer tomographic scans. J Appl Physiol. 2000 Sep;89(3):1013-21.

32. Cole P. Acoustic rhinometry and rhinomanometry. Rhinol Suppl. 2000 Dec;16:29-34.

33. Eccles R. Nasal airflow in health and disease. Acta Otolaryngol. 2000 Aug;120(5):580-95.

34. Cole P. The four components of the nasal valve. Am J Rhinol. 2003 Mar-Apr;17(2):107-10.

35. Farmer SE, Eccles R. Chronic inferior turbinate enlargement and the implications for surgical intervention. Rhinology. 2006 Dec;44(4):234-8.

36. Wang DY, Raza MT, Goh DY, Lee BW, Chan YH. Acoustic rhinometry in nasal allergen challenge study: which dimensional measures are meaningful? Clin Exp Allergy. 2004 Jul;34(7):1093-8.

37. Garcia GJ, Bailie N, Martins DA, Kimbell JS. Atrophic rhinitis: a CFD study of air conditioning in the nasal cavity. J Appl Physiol. 2007 Sep;103(3):1082-92.

38. Wen J, Inthavong K, Tu J, Wang S. Numerical simulations for detailed airflow dynamics in a human nasal cavity. Respir Physiol Neurobiol. 2008 Apr;161(2):125-35.

39. Lee JH, Na Y, Kim SK, Chung SK. Unsteady flow characteristics through a human nasal airway. Respir Physiol Neurobiol. 2010 Jul;172(3):136-46.

40. Cole P. Physiology of the nose and paranasal sinuses. Clin Rev Allergy Immunol. 1998 Spring-Summer;16(1-2):25-54.

41. Hood CM, Schroter RC, Doorly DJ, Blenke EJ, Tolley NS. Computational modeling of flow and gas exchange in models of the human maxillary sinus. J Appl Physiol. 2009 Oct;107(4):1195-203.

42. Naraghi M, Deroee AF, Ebrahimkhani M, Kiani S, Dehpour A. Nitric oxide: a new concept in chronic sinusitis pathogenesis. Am J Otolaryngol. 2007 Sep-Oct;28(5):334-7.

43. Moncada S, Higgs A. The L-arginine-nitric oxide pathway. N Engl J Med. 1993 Dec;329(27):2002-12.

44. Xiong G, Zhan J, Zuo K, Li J, Rong L, Xu G. Numerical flow simulation in the post-endoscopic sinus surgery nasal cavity. Med Biol Eng Comput. 2008 Nov;46(11):1161-7.

45. Bhattacharyya N, Gopal HV, Lee KH. Bacterial infection after endoscopic sinus surgery: a controlled prospective study. Laryngoscope. 2004 Apr;114(4):765-7.

46. Nayak DR, Balakrishnan R. De novo bacterial reinfections after endoscopic sinus surgery: can uncinate process preservation surgeries prevent it? Laryngoscope. 2005 May;115(5):928.

47. Bousquet J, Van Cauwenberge P, Khaltaev N; ARIA Workshop Group; World Health Organization. Allergic rhinitis and its impact on asthma. J Allergy Clin Immunol. 2001 Nov;108(5 Suppl):S147-334.

48. Fokkens W, Lund V, Mullol J; European Position Paper on Rhinosinusitis and Nasal Polyps Group. European position paper on rhinosinusitis and nasal polyps 2007. Rhinol Suppl. 2007;(20):1-136.

49. Senocak D, Senocak M, Bozan S. Sinonasal distribution of topically applied particles: computerized tomographic detection and the effects of topical decongestion. Otolaryngol Head Neck Surg. 2005 Dec;133(6):944-8.

50. Homer JJ, Maughan J, Burniston M. A quantitative analysis of the intranasal delivery of topical nasal drugs to the middle meatus: spray versus drop administration. J Laryngol Otol. 2002 Jan;116(1):10-3.

51. Wenzel A, Henriksen J, Melsen B. Nasal respiratory resistance and head posture: effect of intranasal corticosteroid (Budesonide) in children with asthma and perennial rhinitis. Am J Orthod. 1983 Nov;84(5):422-6.

52. Zhu JH, Lee HP, Lim KM, Lee SJ, Wang DY. Evaluation and comparison of nasal airway flow patterns among three subjects from Caucasian, Chinese and Indian ethnic groups using computational fluid dynamics simulation. Respir Physiol Neurobiol. 2011 Jan;175(1):62-9.

53. Rhee JS, Pawar SS, Garcia GJ, Kimbell JS. Toward personalized nasal surgery using computational fluid dynamics. Arch Facial Plast Surg. 2011 Sep-Oct;13(5):305-10.

54. Pawar SS, Garcia GJ, Kimbell JS, Rhee JS. Objective measures in aesthetic and functional nasal surgery: perspectives on nasal form and function. Facial Plast Surg. 2010 Aug;26(4):320-7.